Dalton Transactions

COMMUNICATION

View Article Online
View Journal | View Issue

Cite this: *Dalton Trans.*, 2015, **44**, 7127

Received 30th January 2015,
Accepted 9th March 2015

DOI: 10.1039/c5dt00429b

www.rsc.org/dalton

Complete surface coverage of ZnO nanorod arrays by pulsed electrodeposited $CuInS_2$ for visible light energy conversion†

Yiming Tang,[a] Jung-Ho Yun,[b] Lianzhou Wang,[b] Rose Amal*[a] and Yun Hau Ng*[a]

Well-aligned ZnO nanorods were uniformly coated with a layer of $CuInS_2$ nanoparticle photosensitizers using a tailored sequential pulsed electrodeposition. The formation of $CuInS_2$–ZnO heterojunction with well-matched band energy alignment and the superior electron mobility in ZnO nanorods led to a remarkable 3.75 times improved photoelectrochemical performance of the electrode under visible light irradiation.

Owing to the distinct electron transport behaviour, one dimensional (1D) nanoarrays of photoactive oxide materials have attracted considerable attention in the design of photovoltaics, liquid state photoelectrochemical cells, and photocatalysis.[1] Semiconducting materials, for example TiO_2, Fe_2O_3, WO_3 and ZnO, have been designed in the form of nanotubes, nanorods, nanowires, nanoneedles and many other 1D-nanostructures,[2] which could be either highly ordered or randomly packed.[3] To extend the light-response of these wide band gap 1D-nanostructured oxides, decoration with narrow bandgap materials as photosensitizers is a popular and effective strategy.[4] Although powders of these oxides can be conveniently coated with binary and ternary photosensitizers (*e.g.* CdS and $CuInS_2$) using hydro (solvo-)thermal method,[5] it remains a great challenge to directly cover the surface of the 1D-nanostructures in the thin film configuration. For thin films, electrodeposition is a simple and effective technique to decorate compact films with a wide range of metallic components, but due to the differences in the deposition kinetics and mechanisms, coating the arrays of well-aligned nanorod and nanotube thin films with secondary components always results in an inadequate coverage of the 1D-nanostructures, and it is mostly limited to the top layer (or entrance) of the 1D-nanostructures. A generally accepted reason is that a gradient of precursor concentration exists throughout the length of the 1D-nanostructures. Higher concentration of the precursor at the top region of the 1D-nanostructures induces rapid nucleation or deposition when cathodic bias is applied. This leads to the immediate formation of the secondary component at the top region (entrance), and subsequently blocks/slows the diffusion of fresh precursor into the deeper region for successive deposition.

$CuInS_2$ is a visible-light-active semiconductor with a chalcogenide-type crystal structure. It demonstrates great potential applications in photovoltaic cells and solar hydrogen cells.[6] Unlike depositing binary sulphides, electrodeposition of the ternary sulphide $CuInS_2$ is more challenging because it involves multi elemental deposition. Therefore, the objective of this study is to uniformly deposit $CuInS_2$ nanoparticles on vertically aligned ZnO nanorod arrays grown on a transparent charge collecting electrode, *i.e.* fluorine-doped tin oxide (FTO) glass substrate. The formation of effective junctions between ZnO and $CuInS_2$ will allow superior charge transfer from the photoexcited $CuInS_2$ to ZnO upon illumination. The charges can be efficiently collected at the charge collecting electrode to improve the charge utilisation. Together with greater light penetration into deeper regions of the 1-D nanostructured film, the pulsed-electrodeposited $CuInS_2$ thin film is expected to show improved photoelectrochemical activities. ZnO nanorod is chosen because it possesses extremely high electron mobility (200–300 $cm^2\ V\ s^{-1}$), a value greater than that of the benchmark set by the semiconductor TiO_2 (0.1–4 $cm^2\ V\ s^{-1}$). Coating ZnO with $CuInS_2$ offers various opportunities in further improving the photoresponse of light-active semiconductors.[7] However, depositing this multi-component $CuInS_2$ on ZnO is challenged by the stability of ZnO in the precursor media with varied pH. Indium (typically $InCl_3$) precursor has a pH value of 3–4, which imposes the gradual dissolution of ZnO during the electrodeposition.[8] A new strategy tailored for ZnO coating with multi-elements (not limited to $CuInS_2$) is therefore in high demand in the area of photoelectrochemical studies.

In this study, we present a square wave sequential pulsed-electrodeposition approach to wrap the ZnO nanorods with

[a]*Particles and Catalysis Research Group, School of Chemical Engineering, The University of New South Wales, Sydney, NSW 2052, Australia. E-mail: r.amal@unsw.edu.au, yh.ng@unsw.edu.au*

[b]*Nanomaterials Centre, School of Chemical Engineering and AIBN, The University of Queensland, QLD 4072, Australia*

†Electronic supplementary information (ESI) available: Experimental details; SEM image of $CuInS_2$–ZnO from non-pulsed electrodeposition and additional PEC measurement of pulsed electrodeposited $CuInS_2$–ZnO under different conditions are involved. See DOI: 10.1039/c5dt00429b

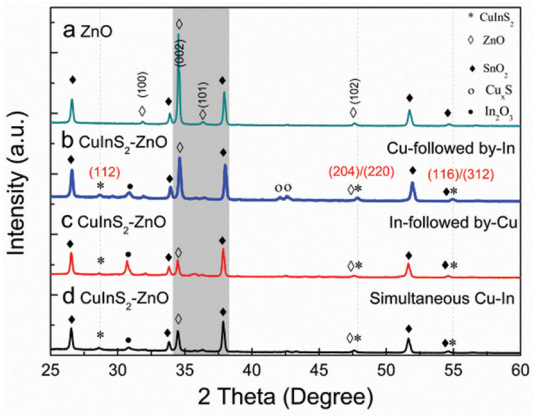

Fig. 1 XRD patterns of the (a) ZnO film and (b–d) $CuInS_2$–ZnO films with various deposition conditions.

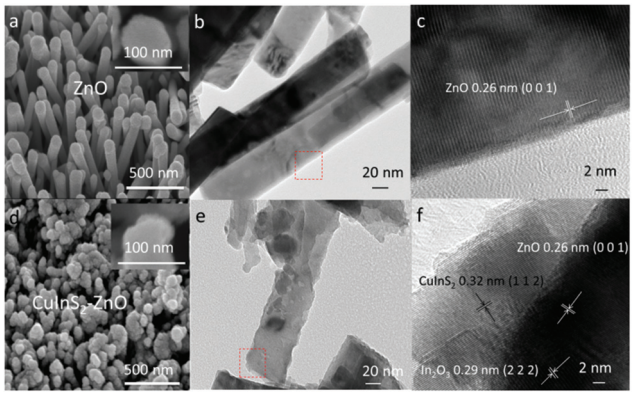

Fig. 2 (a–c) show the surface morphology of ZnO nanorods (+30° tilted view, inset: magnified single ZnO nanorod), TEM image of an individual ZnO nanorod and HRTEM image of the ZnO nanorod, respectively; (d–f) show the surface morphology of CuInSs–ZnO film (+30 tilted view, inset: magnified single $CuInS_2$–ZnO nanorod), TEM image of an individual $CuInS_2$–ZnO nanorod and HRTEM image of the $CuInS_2$–ZnO nanorod.

$CuInS_2$ nanoparticles. The well-aligned ZnO nanorod arrays were prepared using an established chemical bath deposition (CBD) method.[9] Detailed experimental conditions are included in the ESI (Table S1†). X-ray diffraction (XRD) pattern in Fig. 1a shows the successful formation of a crystallized ZnO with the dominant (002) plane on the fluorine-doped tin oxide (FTO) glass substrate. Based on these ZnO nanorods, $CuInS_2$ nanoparticles were pulse-electrodeposited at the frequency of 5 Hz using three different pulsing conditions: (1) Cu deposition followed by In; (2) In deposition followed by Cu; and (3) simultaneous Cu and In deposition. $Na_2S_2O_3$ is always present in the initial pulsed electrodeposition to ensure the incorporation of sulphur component for the subsequent formation of $CuInS_2$ nanocrystals. Fig. 1b–d show the XRD patterns of the resultant $CuInS_2$–ZnO thin films with the abovementioned conditions. All XRD patterns prove the presence of $CuInS_2$ with the main (112) peak at 27.4°.

Noticeably, the peak intensity of ZnO (002) plane relative to the FTO peak was significantly decreased when $CuInS_2$–ZnO was prepared using In-deposition followed by Cu-deposition (Fig. 1c) and simultaneous Cu–In deposition (Fig. 1d). The inductively coupled plasma-atomic emission spectroscopy (ICP-AES) analyses of the post-deposition electrolytes indicate the substantial amount of dissolved Zn in the latter two samples (11.6 ppm for the simultaneous Cu–In deposition; 11 ppm for the In-followed by-Cu deposition), while the Cu deposition followed by In deposition sample shows only mild dissolution of ZnO (0.13 ppm of dissolved Zn). The severity of the ZnO dissolution during the $CuInS_2$ pulsed-electrodeposition was subsequently identified to be related to the pH of the initial precursor solutions. pH 3.8 and pH 3.9 were obtained for the precursor solutions of the simultaneous Cu–In deposition and the In deposition followed by Cu deposition, respectively. The suppression of the ZnO dissolution in the Cu deposition followed by In deposition system was attributed to the ability of thiosulfate ions from $Na_2S_2O_3$ to reduce Cu(II) ions and instantaneously complex with the resulting Cu(I) species. The formation of this stable complex can suppress the release of H^+ from the Cu ion hydrolysis.[10] Therefore, a higher pH value of 6.8 was observed in this system, which resulted in a less substantial ZnO dissolution. No similar complex has been reported for In ions. Cu deposition followed by In deposited $CuInS_2$–ZnO was therefore chosen as the optimized thin film for further investigation.

Fig. 2 shows the scanning electron microscopy (SEM) and transmission electron microscopy (TEM) images of ZnO and $CuInS_2$–ZnO derived from the Cu deposition followed by In deposition sequence. Vertically aligned ZnO nanorods with an average diameter of *ca.* 70 nm were grown on the FTO substrate. TEM images (Fig. 2b and c) with well-defined lattice fringe of 0.26 nm ((001) plane) show highly crystalline ZnO nanorods with a relatively smooth surface, indicating the undecorated morphology of ZnO. Introducing regulated pulsed conditions (5 Hz) in the electrodeposition successfully wrapped the ZnO nanorods evenly with $CuInS_2$ nanoparticles. The slightly thicker and rougher surface of the nanorods (Fig. 2e) indicate the deposition of nanoparticles on ZnO, in which the nanoparticles were identified to be crystalline $CuInS_2$ (Fig. 2f). Note that this uniformly coated ZnO nanorod thin film was rarely seen in the samples prepared with the conventional non-pulsed electrodeposition method.[11] As shown in Fig. S1 (ESI†), non-pulsed electrodeposition led to the formation of a thick $CuInS_2$ layer, only on the top of the ZnO nanorod arrays. Thus, the presence of pulses at an appropriate frequency during the electrodeposition is critical in ensuring the uniform photosensitizer coating on individual nanorods.

It is of interest to discuss the effect of electrodeposition conditions on the formation of $CuInS_2$ coating. The square wave pulse in this study was set at a cathodic bias (−1.25 V, 100 ms) and a relaxation bias (0 V, 100 ms). The nucleation of Cu and In was induced at cathodic bias to form the Cu/In/S intermediate (before the calcination), while the relaxation bias provided sufficient diffusion time for the fresh precursor to reach the un-nucleated sites of ZnO. The repetition of this nucleation-diffusion cycle eventually results in the wrapping of ZnO nanorods with $CuInS_2$ nanoparticles. In contrast, the

non-pulsing condition introduces continuing nucleation energy for the deposition of $CuInS_2$ throughout the deposition. The initial $CuInS_2$ nanoparticles formed on the tip of the ZnO nanorods rapidly grow into a bulky and fused $CuInS_2$ layer, which causes the ultimate blockage of the entrance to the deeper sites of ZnO nanorods. As a result, an ineffective coverage and poor heterojunction of $CuInS_2$–ZnO was formed from the non-pulsed electrodeposition.

Fig. 3a shows the Tauc plots of ZnO and $CuInS_2$–ZnO nanorod arrays. While bare ZnO nanorods demonstrate the typical UV light absorption, $CuInS_2$–ZnO has extended its photoresponse into visible light region. An optical band gap of 1.3 eV was measured on the bare $CuInS_2$ thin film prepared using this method and it is in good agreement with reported values.[6] The considerable absorbance in the window of 390–920 nm reveals the origin of the visible light photocurrent generation, which will be discussed later. In addition to the extended light absorption, electrochemical impedance spectra (EIS) (Fig. 3b) of bare ZnO nanorods, bare $CuInS_2$ film and $CuInS_2$–ZnO film performed under visible light illumination provide useful insight on the bulk conductance of the films. At high frequency (>500 Hz), the conductance of each film is dominated by the electrolyte used in the measurement, and therefore similar values were obtained. The film conductance was indicated in the frequency range from 10 mHz to 500 Hz.[12] The visible light-excited $CuInS_2$–ZnO thin film exhibited the highest conductance compared with the individual component of ZnO film and $CuInS_2$ film. Under visible light, bare ZnO film was not excited; thus, the intrinsic conductance of ZnO was shown. Although the bare $CuInS_2$ film was excited, its limited charge diffusion resulted in moderate bulk conductance. When combined, $CuInS_2$–ZnO film demonstrated superior film conductance because the excited charges from $CuInS_2$ were transferred to ZnO. Owing to the better electron mobility in ZnO, the film conductance is therefore enhanced in the illuminated $CuInS_2$–ZnO.

The constructive effects of extended light absorption and improved film conductance in $CuInS_2$–ZnO nanorods were reflected in their photoelectrochemical current generation. Fig. 3c shows the amperometric photoresponses of ZnO and $CuInS_2$–ZnO nanorod arrays under visible light illumination. $CuInS_2$ is determined to be an n-type semiconductor as it demonstrated anodic photocurrent upon visible light illumination (Fig. S2†). Under illumination with $\lambda > 435$ nm, the $CuInS_2$ component in the composite undergoes charge separation to excite electrons to its conduction band. The difference in energy level between the conduction bands of $CuInS_2$ and ZnO introduces an internal local electric field at the heterojunction that drives the electron transfer from $CuInS_2$ to ZnO.[13] Because ZnO has great electron mobility, the injected electrons are efficiently transported to the external circuit to generate photocurrent. The $CuInS_2$–ZnO nanorod arrays prepared by Cu deposition followed by In deposition sequence show the highest photocurrent density of 1.5 mA cm^{-2}. The photocurrent generation during the on–off illumination cycles was reproducible, although the photoresponses were relatively slow (as indicated by the gradual increase in the current upon

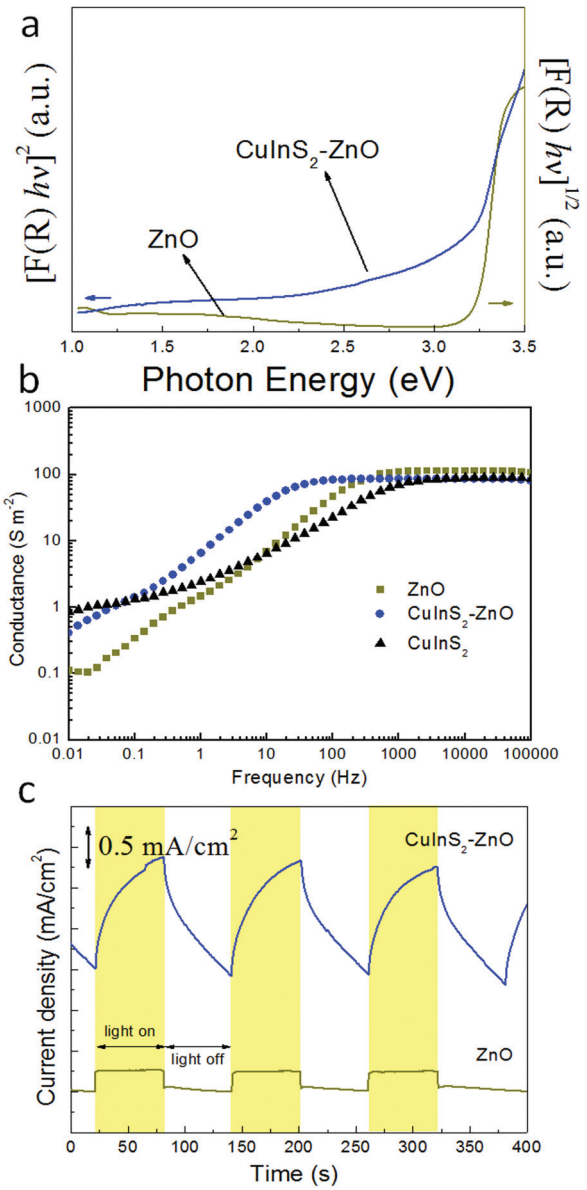

Fig. 3 (a) Tauc plots of ZnO and $CuInS_2$–ZnO arrays prepared by "Cu deposition followed by In deposition" sequence; (b) EIS conductance plots of ZnO and $CuInS_2$–ZnO film prepared by "Cu deposition followed by In deposition" sequence in 0.1 mol L^{-1} lithium perchlorate ($LiClO_4$) in acetonitrile (CH_3CN) solution under visible light illumination; (c) photocurrent response of ZnO and $CuInS_2$–ZnO film prepared by "Cu deposition followed by In deposition" method at 0.75 V *vs.* Ag/AgCl in an electrolyte containing 0.25 mol L^{-1} Na_2S and 0.35 mol L^{-1} Na_2SO_3 (pH = 12) under visible light irradiation ($\lambda \geq 435$ nm).

illumination) compared with oxide-based photoactive films due to its slower electron transfer kinetics.[14] For comparison, $CuInS_2$–ZnO nanorod arrays derived from the simultaneous Cu–In deposition and In deposition followed by Cu deposition sequence only generated 0.6 and 0.4 mA cm^{-2}, respectively (see Fig. S3 in ESI†). The lower photocurrent generated in these two samples is attributed to two reasons: (i) severe dissolution of ZnO component during $CuInS_2$ deposition as evidenced by the lower XRD peak for ZnO together with the

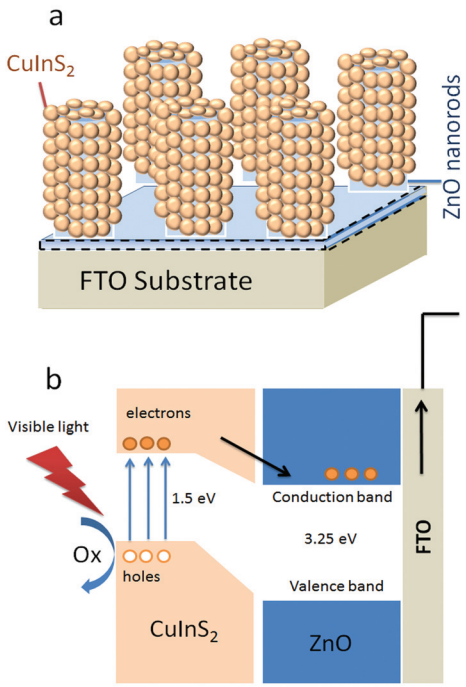

Fig. 4 (a) Schematic diagram of the $CuInS_2$–ZnO film; (b) electronic structures of $CuInS_2$–ZnO film.

dissolved ZnO measured by ICP, and (ii) the formation of In_2O_3 as impurities at the interface of the composite as can be seen in the HRTEM image (Fig. 2f). These results highlight the importance of tailoring the deposition condition according to the specific properties of the host materials (ZnO nanorods in this work and TiO_2 nanotubes in our previous report[4]). Photocurrent density of 0.25 mA cm^{-2} was observed in the bare ZnO nanorods and the excitation is attributed to the remnant UV component of the incident light that passed through the optical cut-off filter.[15]

Schematic illustration of $CuInS_2$–ZnO structure (Fig. 4a) depicts the close vicinity and effective contact between $CuInS_2$ nanoparticles and ZnO nanorods derived from the sequential pulsed-electrodeposition. The well-matched band alignment of these two components, as shown in Fig. 4b, also promotes the transfer of excited electrons from $CuInS_2$. Lastly, the superior electron mobility in ZnO allows the efficient transportation of the injected charge to be utilized at the counter electrode.

In summary, a tailored deposition sequence was found to be influential in fabricating $CuInS_2$–ZnO nanorods with effective heterojunction. The square wave pulsed condition was the key factor leading to a complete coating of the ZnO nanorods with an even layer of $CuInS_2$ nanoparticles. A high quality heterojunction further empowered by the energetically favoured band alignment facilitated good photoelectrochemical performances.

Acknowledgements

This work has been supported by the Australian Research Council Discovery Project (DP110101638). Yiming Tang also acknowledges the scholarship under the State Scholarship Fund awarded by China Scholarship Council. The authors would also like to acknowledge the UNSW Mark Wainwright Analytical Centre, and particularly thank Dr Katie Levick for her generous help in the TEM analysis.

Notes and references

1 (*a*) K. Kiatkittipong, J. Scott and R. Amal, *ACS Appl. Mater. Interfaces*, 2011, **3**, 3988; (*b*) C. M. Johnson, P. J. Reece and G. J. Conibeer, *Opt. Lett.*, 2011, **36**, 3990; (*c*) J. Xiong, Z. Li, J. Chen, S. Zhang, L. Wang and S. Dou, *ACS Appl. Mater. Interfaces*, 2014, **6**, 15716.

2 (*a*) Y. Bai, H. Yu, Z. Li, R. Amal, G. Q. Lu and L. Wang, *Adv. Mater.*, 2012, **24**, 5850; (*b*) J.-H. Yun, Y. H. Ng, C. Ye, A. J. Mozer, G. G. Wallace and R. Amal, *ACS Appl. Mater. Interfaces*, 2011, **3**, 1585; (*c*) Y. Ling, G. Wang, D. A. Wheeler, J. Z. Zhang and Y. Li, *Nano Lett.*, 2011, **11**, 2119; (*d*) C. Ng, C. Ye, Y. H. Ng and R. Amal, *Cryst. Growth Des.*, 2010, **10**, 3794; (*e*) M. Law, L. E. Greene, J. C. Johnson, R. Saykally and P. Yang, *Nat. Mater.*, 2005, **4**, 455.

3 S. Xu and Z. Wang, *Nano Res.*, 2011, **4**, 1013.

4 J.-H. Yun, Y. H. Ng, S. Huang, G. Conibeer and R. Amal, *Chem. Commun.*, 2011, **47**, 11288.

5 (*a*) F. Shen, W. Que, Y. He, Y. Yuan, X. Yin and G. Wang, *ACS Appl. Mater. Interfaces*, 2012, **4**, 4087; (*b*) Y. Li, Z. Liu, Y. Wang, Z. Liu, J. Han and J. Ya, *Int. J. Hydrogen Energy*, 2012, **37**, 15029.

6 (*a*) Y. Tang, Y. H. Ng, J.-H. Yun and R. Amal, *RSC Adv.*, 2014, **4**, 3278; (*b*) F. M. Courtel, A. Hammami, R. Imbeault, G. Hersant, R. W. Paynter, B. Marsan and M. Morin, *Chem. Mater.*, 2010, **22**, 3752.

7 U. Özgür, Y. I. Alivov, C. Liu, A. Teke, M. A. Reshchikov, S. Doğan, V. Avrutin, S. J. Cho and H. Morkoç, *J. Appl. Phys.*, 2005, **98**, 041301.

8 (*a*) S. Sanchez, D. Aldakov, D. Rouchon, L. Rapenne, A. Delamoreanu, C. Levy-Clement and V. Ivanova, *J. Renewable Sustainable Energy*, 2013, **5**, 011207; (*b*) S. Peulon and D. Lincot, *J. Electrochem. Soc.*, 1998, **145**, 864.

9 L. Vayssieres, K. Keis, S.-E. Lindquist and A. Hagfeldt, *J. Phys. Chem. B*, 2001, **105**, 3350.

10 T. Yukawa, K. Kuwabara and K. Koumoto, *Thin Solid Films*, 1996, **280**, 160.

11 S. Sanchez, D. Aldakov, D. Rouchon, L. Rapenne, A. Delamoreanu, C. Levy-Clement and V. Ivanova, *J. Renewable Sustainable Energy*, 2013, **5**, 011207.

12 N. J. Bell, Y. H. Ng, A. Du, H. Coster, S. C. Smith and R. Amal, *J. Phys. Chem. C*, 2011, **115**, 6004.

13 (*a*) T. L. Li, Y. L. Lee and H. S. Teng, *J. Mater. Chem.*, 2011, **21**, 5089; (*b*) R. Loef, J. Schoonman and A. Goossens, *J. Appl. Phys.*, 2007, **102**, 024512.

14 Y. H. Ng, A. Iwase, N. J. Bell, A. Kudo and R. Amal, *Catal. Today*, 2011, **164**, 353.

15 Y. Choi, M. Beak and K. Yong, *Nanoscale*, 2014, **6**, 8914.